

Light storage for one second at room temperature

Or Katz^{1,2,*} and Ofer Firstenberg¹

¹*Department of Physics of Complex Systems, Weizmann Institute of Science, Rehovot 76100, Israel*

²*Rafael Ltd, IL-31021 Haifa, Israel*

Light storage, the controlled and reversible mapping of photons onto long-lived states of matter [1], enables memory capability in optical quantum networks [2–6]. Prominent storage media are warm alkali gases due to their strong optical coupling and long-lived spin states [7, 8]. In a dense gas, the random atomic collisions dominate the lifetime of the spin coherence, limiting the storage time to a few milliseconds [9, 10]. Here we present and experimentally demonstrate a storage scheme that is insensitive to spin-exchange collisions, thus enabling long storage times at high atomic densities. This unique property is achieved by mapping the light field onto spin orientation within a decoherence-free subspace of spin states. We report on a record storage time of 1 second in cesium vapor, a 100-fold improvement over existing storage schemes. Furthermore, our scheme lays the foundations for hour-long quantum memories using rare-gas nuclear spins.

The archetypal mechanism of light storage is based on electromagnetically induced transparency (EIT), involving the *signal* field to be stored and a strong *control* field [11–14]. These fields resonantly couple one atomic excited state to two spin states within the ground level. Under EIT, there exists a long-lived dark state, which is the superposition of these spin states that is decoupled from the excitation pathways. While the control is on, the signal pulse entering the medium couples coherently to the dark state, forming a slowly-propagating polariton. Storage is done by turning off the control and stopping the polariton, thereby mapping the signal field onto a stationary field of dark-state coherence. Turning on the control retrieves the signal.

In addition to the electron spin $S = 1/2$, alkali-metal atoms have a nuclear spin $I > 0$ ($I = 7/2$ for ^{133}Cs) and thus possess multiple spin states. These are characterized by the hyperfine spin $F = I \pm S$ and its projection m on the quantization axis \hat{z} . Various combinations of spin states are accessible with different signal-control configurations, as shown in Fig. 1. Most light storage schemes utilize either the Zeeman coherence $\Delta m = 2$ (Fig. 1a) or the hyperfine coherence $\Delta m = 0$ (Fig. 1b) [10]. The relaxation of these coherences at high atomic densities is dominated by pairwise spin-exchange collisions [15]. During a collision, the valence electrons of the colliding pair overlap for a few picoseconds, accumulating a phase between the hybridized (singlet and triplet) electronic spins. While the total spin is conserved, the randomness of the collision parameters leads to relaxation of most ground-state coherences, limiting the storage lifetime in these schemes [11, 16].

It has been known, however, that the Zeeman coherence $\Delta m = 1$, associated with the spin orientation moment, is unaffected by spin-exchange collisions at low

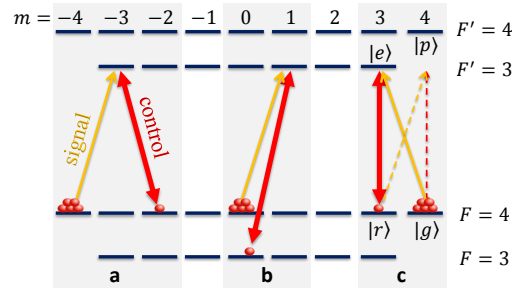


Figure 1. **Configurations of light storage on the cesium ground-level.** **a**, Zeeman coherence $|\Delta m| = 2$. **b**, Hyperfine coherence $|\Delta m| = 0$. **c**, Zeeman coherence $|\Delta m| = 1$, associated with spin orientation, used here. The dashed arrows represent an additional weak process, discussed in the text. Note that the signal is stored and retrieved as a linearly-polarized field, despite the fact that only one of its circular-polarization components (solid yellow line) enters the A -system $|g\rangle - |e\rangle - |r\rangle$, see Methods.

magnetic fields [17, 18]. This property is the underlying principle of spin-exchange relaxation-free (SERF) magnetometers, currently the most sensitive magnetic sensors [19, 20]. Here we realize SERF light storage, closely related to the idea of a SERF atomic clock [21], by mapping the signal onto the $\Delta m = 1$ coherence (Fig. 1c).

A paraffin-coated vapor cell is at the heart of the experimental system, shown in Fig. 2a. We zero the magnetic field to better than $|B| < 1 \mu\text{G}$ and control the cesium density $n(T)$ via the cell temperature T . The experimental sequence is shown in Fig. 2b. We initially orient the atoms along the optical axis \hat{x} using optical pumping (polarization $> 95\%$). We then rotate the polarized spins onto our quantization axis \hat{z} using a short pulse of magnetic field along \hat{y} , thus preparing them in the state $|g\rangle \equiv |F = 4, m = 4\rangle$. Subsequently, we turn on the control field and a small magnetic field

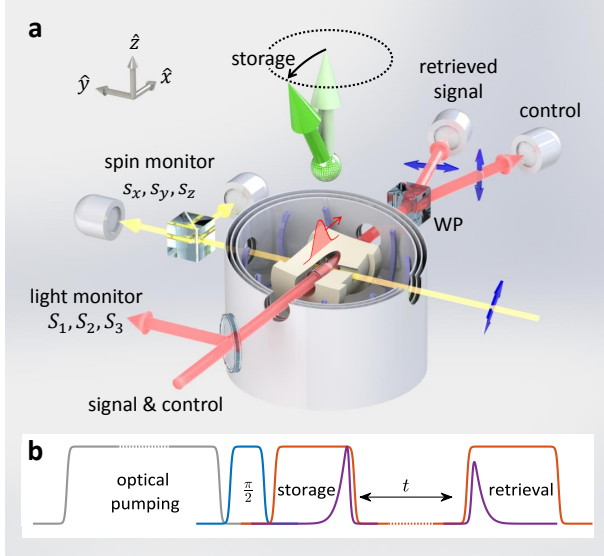


Figure 2. Experimental setup and sequence. A cylindrical vapor cell with diameter 10 mm and length 30 mm is held inside a hot-air oven (a, beige), enclosed by three Helmholtz coil pairs and magnetic shield layers. First, optical pumping (b, gray) is done along \hat{x} using two circularly-polarized beams (not shown in a) for the two hyperfine sub-levels. Subsequently, a $\pi/2$ pulse of magnetic field along \hat{y} (b, blue) prepares a spin ensemble oriented along \hat{z} (a, light green arrow). The control and incoming signal (a, red beam) are sampled before the cell to monitor their polarization state. Storage and retrieval of a signal pulse (b, purple) is done by turning off and then on the control (b, red). The light state is stored onto the orientation of the tilted spin polarization (a, dark green arrow), which can be monitored with auxiliary far-detuned light (a, yellow beam). The retrieved signal is separated from the control using a high extinction-ratio Wollaston prism (WP). Blue arrows in (a) indicate optical polarizations.

$B_z \leq 15 \mu\text{G}$. The control field is linearly polarized along \hat{z} and resonant with the $|r\rangle = |F=4, m=3\rangle \rightarrow |e\rangle = |F'=3, m'=3\rangle$ transition.

With the control on, we send a weak signal pulse, linearly polarized along \hat{y} . The signal couples to the $|g\rangle - |r\rangle$ coherence, orienting the spins while propagating. We store the signal field onto spin orientation by turning off the control and, after a duration t , retrieve it by turning the control back on. As a reference, we perform light storage in a standard $\Delta m = 2$ scheme [11]. At a density of $n = 1.4 \times 10^{11} \text{ cm}^{-3}$ ($T \approx 40^\circ \text{C}$), the two schemes exhibit comparable (internal) storage efficiency, on order 10%, with no particular optimization of the temporal shape of the control and signal [16]. Figures 3a,b show the retrieved pulses for both schemes. We extract the storage lifetime τ_s by fitting the retrieved power to the decay function $\exp(-t/\tau_s)$. Light storage on spin orientation exhibits a remarkable

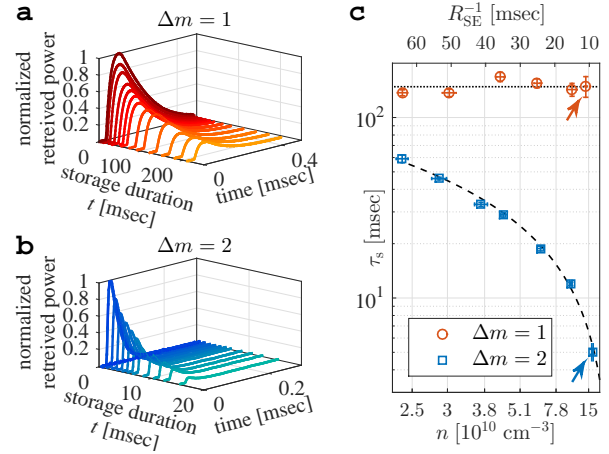


Figure 3. Storage lifetime. a,b, Retrieved pulses for several storage durations in our scheme $\Delta m = 1$ (a), compared to the standard scheme $\Delta m = 2$ (b). The lifetime in our scheme is longer than 100 msec, compared to only a few msec in the standard scheme. c, Storage lifetime as a function of atomic density n and spin-exchange rate R_{SE} in our scheme (red), which is unaffected by collisions and thus remains constant (dotted line). In contrast, the lifetime of the standard scheme (blue) is well described by a linear fit (dashed line). Data in (a,b) correspond to points marked by arrows in (c). The two schemes exhibit comparable storage lifetimes only at low atomic densities, where the optical depth and thus the storage efficiency are compromised [1].

lifetime $\tau_s = 149(20)$ msec in this experiment, much longer than the $5.0(3)$ msec obtained with the standard scheme.

To study the effect of spin-exchange collisions, we tune the collision rate $R_{SE} = \alpha n(T)$ by changing T ($\alpha = 6.5 \cdot 10^{-10} \text{ cm}^3/\text{sec}$ near room temperature) [22]. Figure 3c shows the measured storage lifetime versus R_{SE} . The relaxation of the $\Delta m = 2$ coherence is dominated by spin exchange, as indicated by the linear dependence of τ_s on R_{SE} in the standard scheme. In contrast, our scheme is found to be insensitive to R_{SE} , affirming that the $\Delta m = 1$ coherence is conserved under spin exchange. We conclude that storage on spin orientation maintains long memory lifetimes at elevated optical depths. The observed lifetime $\tau_s = 150$ msec is limited by the spin-destruction time at low magnetic fields, measured $T_1 = 300 \pm 100$ msec in our system.

We confirm the coherent nature of our storage scheme by measuring for $t = 100$ msec the phases of the input signal ϕ_L and output signal ϕ_L^{out} , as shown in Fig. 4a. Larmor precession during storage leads to a constant offset between ϕ_L^{out} and ϕ_L . The Larmor frequency in this experiment was measured independently to be $\omega_B = 1.34(6) \cdot 2\pi$ Hz, predicting a rotation of $\omega_B t = 0.84(4)$, in agreement with the observed offset $\phi_L - \phi_L^{\text{out}} = 0.9(2)$.

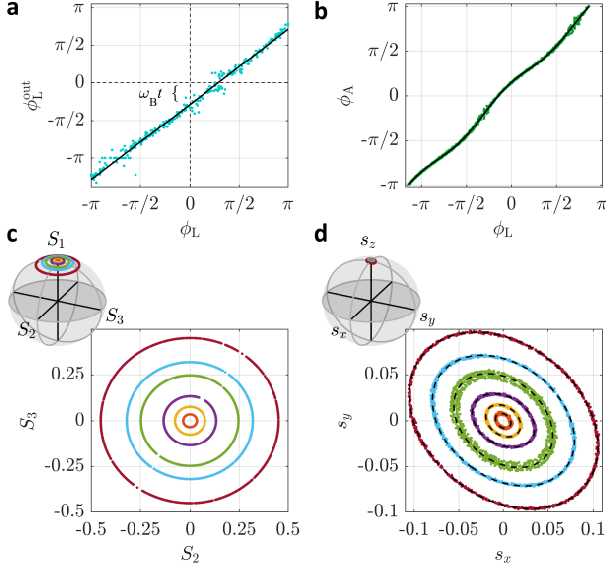


Figure 4. Mapping from light polarization to spin orientation and back. **a**, The measured phase of the retrieved light after storage for $t = 100$ msec follows the input phase up to an offset (line is a linear fit with unity slope). **b**, The azimuthal angle of the collective atomic spin versus the incoming optical phase (line is a fit to elliptical mapping). **c**, Light polarization visualized on the Poincaré sphere and projected onto the transverse plane. **d**, Collective atomic spin visualized on the Bloch sphere and projected onto the transverse plane. Data in **b-d** taken 1 msec after storage (without retrieval).

To explain the immunity to spin-exchange collisions, we first explore the light-atom mapping. Taking the control field as a phase reference, the signal properties, or the light ‘state’ to be stored, are encompassed in the polarization of the incoming (signal+control) field. This polarization is visualized on the Poincaré sphere using the Stokes parameters S_1, S_2, S_3 in Fig. 4c. To characterize their mapping onto the atomic spins, we monitor the spins during storage using polarization rotation of a far-detuned beam. The spin state of the ensemble is described by the collective electronic spin $\vec{s} = (s_x, s_y, s_z)$, defined by $\vec{s} = \frac{1}{N} \sum_i \langle \vec{s}^i \rangle$, where \vec{s}^i is the spin operator of the i^{th} atom and N the number of atoms [23]. These are visualized on the Bloch sphere in Fig. 4d.

From the Stokes operators, we extract for the light the complex ratio $i\eta_L e^{i\phi_L} = E_s/E_c$ between the signal amplitude E_s and the control amplitude E_c . The phase ϕ_L is constant in space and time during an experimental sequence. As the signal is much weaker than the control $\eta_L \ll 1$, the Stokes vector is located near the north pole of the Poincaré sphere (Fig. 4c). Initially, with only the control on ($\eta_L = 0$), the atomic spins are oriented along the \hat{z} direction, corresponding to the north pole of the Bloch sphere. This initialized spin orientation underlies

the difference between our system and those previously demonstrated with the same fields configuration [10, 12, 24]. The incoming signal tilts the collective spin off the pole, producing transverse spin components (Fig. 4d).

The light state has a polar angle η_L and an azimuth ϕ_L ; the corresponding atomic state has a polar angle $\eta_A = \sqrt{s_x^2 + s_y^2}/s_z$ and azimuth $\phi_A = \arctan(s_y/s_x)$. We find that the storage procedure maps the light quadratures S_2, S_3 onto the spin components s_y, s_x by transforming circles into nearly-circular ellipses with $\phi_A \approx \phi_L$, see Fig. 4b. We conclude that the light state is mapped onto the atomic spin orientation.

The immunity to spin-exchange collisions can easily be understood in the absence of hyperfine interaction (*e.g.* if $I = 0$), as the total spin, and hence the orientation of the electronic spin, is conserved under these collisions. However when $I > 0$, it is not trivial to see how also the entanglement between the electronic and nuclear spins is conserved. To understand the case $I > 0$, we examine a collision between two cesium atoms. After a weak classical signal is stored, the state of the i^{th} atom is $|\psi_i\rangle = |g_i\rangle + \sqrt{2}\eta_A e^{i\phi_A} |r_i\rangle$, with $\eta_A \ll 1$. The collision is brief relatively to the hyperfine frequency and thus affects only the electronic spins. We therefore decompose the stored state into the electronic $|\uparrow_i\rangle \equiv |s_z^i = \frac{1}{2}\rangle$, $|\downarrow_i\rangle \equiv |s_z^i = -\frac{1}{2}\rangle$ and nuclear $|\uparrow_i\rangle \equiv |I_z^i = I\rangle$, $|\downarrow_i\rangle \equiv |I_z^i = I-1\rangle$ spin components, writing $|\psi_i\rangle = |\uparrow_i\uparrow_i\rangle + \sqrt{2}\eta_A e^{i\phi_A} (q|\uparrow_i\downarrow_i\rangle + p|\downarrow_i\uparrow_i\rangle)$. For cesium, $I = \frac{7}{2}$ and $p^2 = 1 - q^2 = \frac{1}{8}$ (note that the following arguments are general and independent of these values). The exchange interaction during a collision between a pair of atoms introduces a random phase χ between their hybrid electronic states – the singlet and triplet [15]. The pair, initially in the product state $|\psi_{ij}\rangle = |\psi_i\rangle |\psi_j\rangle$, leaves the collision in the state $(P_T^{i,j} + e^{i\chi} P_S^{i,j}) |\psi_{ij}\rangle$, where $P_S^{i,j} = (|\uparrow_i\downarrow_j\rangle - |\downarrow_i\uparrow_j\rangle)(\langle\uparrow_i\downarrow_j| - \langle\downarrow_i\uparrow_j|)/2$ and $P_T^{i,j} = 1 - P_S^{i,j}$ are the singlet and triplet projection operators. Yet for weak signals, at the limit $\eta_A \rightarrow 0$, the colliding pair is a nearly-perfect spin triplet, possessing a negligible singlet component $\langle\psi_{ij}| P_S^{i,j} |\psi_{ij}\rangle = 4(pq)^2 \eta_A^4 \rightarrow 0$ [21]. Therefore, the random phase χ is inconsequential, and the pair state is immune to spin-exchange relaxation.

It is also instructive to examine the quantum limit, where the signal has at most a single photon in the state $\alpha|0\rangle + \beta|1\rangle$, where α and β are the SU(2) parameters of a qubit with either zero $|0\rangle$ or one $|1\rangle$ photons. At storage, the initial collective atomic state $|G\rangle = \prod_i |g_i\rangle$ is transformed into $|R\rangle = (\alpha + \beta F_-)|G\rangle$, where $F_- = \frac{1}{N} \sum_i (s_-^i + i_-^i)$ is the collective spin operator accounting for the $\Delta m = 1$ transition. One can verify that $|R\rangle$ is an exact triplet for any atom pair (i, j) , since $|G\rangle$ is a triplet and $[P_T^{i,j}, F_-] = 0$. Therefore, the stored qubit

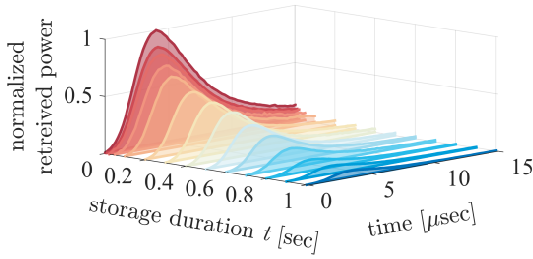


Figure 5. Light storage for up to $t = 1$ sec of short ($\tau_p = 5.5 \mu\text{sec}$) signal pulses.

$|R\rangle$ is fully conserved under spin exchange.

Finally, we note that a mapping $\eta_L e^{i\phi_L} \leftrightarrow \eta_A e^{i\phi_A}$ with nonzero ellipticity is non-ideal for quantum memories, as it links the retrieval amplitude to the (azimuthal) phase and thus distorts the quantum state. In our experiment, the ellipticity originates from polarization self-rotation [25] due to the off-resonance Raman process $|g\rangle - |p\rangle - |r\rangle$ (dashed arrows in Fig. 1c) weakly perturbing the ideal EIT process $|g\rangle - |e\rangle - |r\rangle$. When the strength of these processes is comparable, the resulting so-called Faraday interaction limits the storage to *only* one quadrature, compressing the ellipse into a line [23]. In our scheme, $\Delta > \Gamma$, where Δ and Γ are the detuning and Doppler-linewidth of the $|g\rangle - |p\rangle$ transition, so the dark state qualitatively obtains the form $|g\rangle + \sqrt{2}\eta_L (e^{i\phi_L} - \epsilon e^{-i\phi_L}) |r\rangle$, with $\epsilon = (1 - i\Delta/\Gamma)^{-1}$; in cesium, $\Delta \approx 10\Gamma$, yielding ellipticity of order 0.1. An ideal mapping $\epsilon \rightarrow 0$ with $\Delta \gg \Gamma$ is possible, *e.g.*, by storing on the lower hyperfine ground-level ($|r\rangle \Rightarrow |F=4, m=3\rangle$), which still maintains the spin-exchange resistance. We derive in the SI the exact analytical form of the mapping $\eta_L e^{i\phi_L} \leftrightarrow \eta_A e^{i\phi_A}$ and further develop a procedure employing a magnetic field B_z that corrects for and eliminates the ellipticity. It follows that the ellipticity is non-fundamental and amendable.

Upon completion of the measurements reported above, we kept the vapor cell warm at $T = 45^\circ\text{C}$ for a week, keeping the stem cold at $T = 25^\circ\text{C}$, and performed storage experiments for up to $t = 1$ sec. As shown in Fig 5, we observed a $1/e$ storage time of $\tau_s = 430(50)$ msec, indicating that the temperature cycle lowered the spin destruction, presumably due to “curing” of the coating [26]. In conjunction with the signal pulse duration of $\tau_p = 5.5 \mu\text{sec}$, we thus obtained an extremely large fractional delay of $\tau_s/\tau_p \approx 80,000$.

In conclusion, our light-storage scheme demonstrates record lifetimes of hundreds of msec at room temperature. In addition, it paves the way towards the coupling of photons to ultra-stable nuclear spins. Rare isotopes of noble gases, such as helium-3, carry nuclear spins that are optically inaccessible and exhibit coherence times on

the scale of hours [27]. It has been demonstrated that spin-exchange collisions can *coherently* couple the orientation moment of two alkali species [28, 29] as well as the orientation moment of alkali and rare-gas atoms [30], while all other spin moments are relaxed. Mapping light onto spin *orientation* thus not only protects the stored information from self spin-exchange relaxation, but also enables its transfer from one spin ensemble to another. Therefore, combined with coherent spin-exchange interaction between alkali and rare gases, our scheme is potentially a key element in employing and manipulating nuclear spins for quantum information applications.

ACKNOWLEDGMENTS

We thank O. Peleg, C. Avinadav, and R. Shaham for helpful discussions and M. Sturm and P. Fierlinger for providing us the vapor cell. We acknowledge financial support by the Israel Science Foundation and ICORE, the European Research Council starting investigator grant Q-PHOTONICS 678674, the Minerva Foundation, the Sir Charles Clore research prize, and the Laboratory in Memory of Leon and Blacky Broder.

METHODS

Experimental calibration.— We perform calibration experiments prior to storage, adjusting the setup parameters to produce no output signal in the absence of an incoming signal. In particular, we fine tune the spin rotation from \hat{x} to \hat{z} after optical pumping and zero the transverse magnetic fields (B_x and B_y). This calibration is important, as light storage based on $|\Delta m| = 1$ coherence is particularly sensitive to experimental imperfections affecting the collective spin orientation: Nonzero transverse magnetic fields ($B_x, B_y \neq 0$) tilt the collective spin during storage and produce a small transverse spin component, which is subsequently mapped to an output signal even without an input signal. Additionally, misalignment between the direction of the (linear) polarization of the control field and the initial polarization direction of the spin ensemble manifests as a nonzero transverse spin (when identifying the control polarization as the quantization axis), again producing an output signal for no input signal. We thus properly align the initial spin polarization direction and validate that B_x and B_y are truly zeroed by verifying the absence of output signal for all “storage” durations t , confirming that there is absolutely no tilt of the spin during the experiment.

Phase uniformity.— In the storage experiments, we send weak signal pulses of durations $\tau_p = 0.03\text{--}0.15$ ms,

linearly polarized along \hat{y} , and having the same spatial mode and frequency as the control field. The corresponding range of pulse bandwidths $2\tau_p^{-1} \approx 2 - 10 \cdot 2\pi$ kHz is comparable to the width of the EIT transmission window and much larger than the Larmor precession rate ω_B , such that the relative phase between the signal and control fields is constant during a storage experiment. The signal and control beams cover the entire cell volume, with their wave-vector difference much smaller than the inverse cell width. This was chosen, because the storage lifetime is sensitive to the spatial-mode overlap of the signal and control fields. Specifically, an angular deviation between them yields a spatial phase grating, which is imprinted on the collective spin wave. Dephasing of this spin wave due to thermal atomic motion limits the storage lifetime [31], as it does regardless of the exact spin coherence used. However for the $|\Delta m| = 1$ scheme, the spin-wave grating manifests as a spatially varying orientation, impairing the resistance to spin-exchange collisions. Colliding spins with different orientations are no longer perfect triplets (the singlet component $\langle \psi_{ij} | P_S^{i,j} | \psi_{ij} \rangle$ grows quadratically with the angle between the colliding spins), which can be explained by their reduced indistinguishability due to the spatially-varying mapping. Consequently, the $|\Delta m| = 1$ scheme would lose its SERF property were the signal and control beams misaligned.

Completeness of the $|\Delta m| = 1$ transition.— It is instructive to discuss an intricacy that arise when the quantization axis (\hat{z}) is orthogonal to the light propagation axis (\hat{x}) in the special case of an ensemble initially polarized (oriented) along \hat{z} . With a control field linearly-polarized along \hat{z} , the maximally-polarized atoms are confined to a single $|\Delta m| = 1$ transition. From the viewpoint of the quantization axis \hat{z} , this transition corresponds to the Λ -system $|g\rangle - |e\rangle - |r\rangle$, as depicted in Fig. 1. Importantly, the signal mode is completely stored and retrieved via this transition, despite the fact that its linear polarization (\hat{y}) decomposes to two circular polarizations, of which only one is included in the $|g\rangle - |e\rangle - |r\rangle$ system. Under the reduced Maxwell equations, including the transverse susceptibility tensor of the medium [22], the normal modes comprises only E_y and E_z components (recall that the non-evanescent field polarization remains within the transverse plane during praxial propagation). Consequently, the signal mode E_y is stored and retrieved ‘as a whole’. The optical depth for the signal is however reduced by the Clebsch-Gordan coefficient of the $|g\rangle - |e\rangle$ transition.

Measuring light and spin polarizations.— To measure the Stokes parameters of the light and extract η_L and ϕ_L , we sample the optical fields before the cell. To measure the collective atomic spin, we use a weak monitor beam propagating along \hat{y} , linearly polarized (\hat{z}) and

red-detuned 22 GHz from the $|g\rangle \rightarrow |e\rangle$ transition. Far from resonance, the polarized atoms render the medium optically chiral, rotating the polarization of the monitor beam in the xz plane by an angle $\theta = \beta s_y$ via the linear Faraday interaction, where β is a constant [22]. We measure θ after the cell using a balanced detector [29]. The collective spin during storage is measured by increasing the magnetic field to $B_z = 4$ mG, making the spin precess around the \hat{z} axis at a frequency $\omega_B = 1.4 \cdot 2\pi$ kHz and thus modulating θ in time according to $\theta = C \cos(\omega_B t + \phi_A)$. We identify the transverse spin components at storage as $s_x = C \cos(\phi_A) / \beta$ and $s_y = C \sin(\phi_A) / \beta$. We scan the input phase ϕ_L at various signal powers and measure s_x, s_y in each realization. We perform an additional set of experiments by applying B_x instead of B_z , thus modulating the spin in the yz plane and measuring $\overline{s_z}$ averaged per signal power. With s_x, s_y , and $\overline{s_z}$, we extract $\eta_A = \sqrt{s_x^2 + s_y^2} / \overline{s_z}$ and $\phi_A = \arctan(s_y / s_x)$. For each measurement, we use the normalized vector $\vec{s} / \|\vec{s}\|$ to lay the spin on the Bloch sphere and eliminate β , which is independent of the signal parameters [22].

* Corresponding author: or.katz@weizmann.ac.il

- [1] Lukin, M. D. Colloquium: Trapping and manipulating photon states in atomic ensembles. *Rev. Mod. Phys.* 75, 457–472 (2003).
- [2] O’Brien, J. L. Optical quantum computing. *Science* 318, 1567–1570 (2007).
- [3] Heshami K., Englanda D. G., Humphreys P. C., Bustarda P. J., Acostac V. M., Nunn J. & Sussman B. J. Quantum memories: emerging applications and recent advances. *J. Mod. Opt.* 63, 2005–2028 (2016).
- [4] Lvovsky, A. I., Sanders, B. C. & Tittel, W. Optical quantum memory. *Nature Photon.* 3, 706–714 (2009).
- [5] Sangouard, N., Simon, C., De Riedmatten, H. & Gisin, N. Quantum repeaters based on atomic ensembles and linear optics. *Rev. Mod. Phys.* 83, 33–80 (2011).
- [6] Finkelstein R., Poem E., Michel O., Lahad O. & Firstenberg O. Fast, noise-free memory for photon synchronization at room temperature, arXiv:1708.01919 (2017).
- [7] Hammerer, K., Sørensen, A. S. & Polzik, E. S. Quantum interface between light and atomic ensembles. *Rev. Mod. Phys.* 82, 1041–1093 (2010).
- [8] Hosseini M., Sparkes B. M., Campbell G., Lam P. K. & Buchler B. C. High efficiency coherent optical memory with warm rubidium vapour. *Nat. Commun.* 2, 174 (2011).
- [9] Cho Y.-W., Campbell G. T., Everett J. L., Bernu J., Higginbottom D. B., Cao M. T., Geng J., Robins N. P., Lam P. K. & Buchler B. C. Highly efficient optical quantum memory with long coherence time in cold atoms, *Optica* 3, 100–107 (2016).
- [10] Novikova, I., Walsworth, R. & Xiao, Y. Electromagnetically induced transparency-based slow and stored light

- in warm atoms. *Laser Photon. Rev.* 6, 333–353 (2012).
- [11] Phillips, D. F., Fleischhauer, A., Mair, A., Walsworth, R. L. & Lukin, M. D. Storage of light in atomic vapor. *Phys. Rev. Lett.* 86, 783–786 (2001).
 - [12] Karpa L., Vewinger F. & Weitz M. Resonance Beating of Light Stored Using Atomic Spinor Polaritons. *Phys. Rev. Lett.* 101, 170406 (2008).
 - [13] Novikova I., Phillips D. F. & Walsworth R. L. Slow Light with Integrated Gain and Large Pulse Delay. *Phys. Rev. Lett.* 99, 173604 (2007).
 - [14] Schraft D., Hain M., Lorenz N. & Halfmann T. Stopped Light at High Storage Efficiency in a $\text{Pr}^{3+} : \text{Y}_2\text{SiO}_5$ Crystal. *Phys. Rev. Lett.* 116, 073602 (2016).
 - [15] Happer, W. Optical pumping. *Rev. Mod. Phys.* 44, 169–249 (1972).
 - [16] Phillips, N. B., Gorshkov, A. V. & Novikova, I. Optimal light storage in atomic vapor. *Phys. Rev. A* 78, 023801 (2008).
 - [17] Happer, W. & Tang, H. Spin-exchange shift and narrowing of magnetic resonance lines in optically pumped alkali vapors. *Phys. Rev. Lett.* 31, 273–276 (1973).
 - [18] Katz, O. Dikopoltsev M., Peleg O., Shuker M., Steinhauer J. & Katz N. Nonlinear elimination of spin-exchange relaxation of high magnetic moments. *Phys. Rev. Lett.* 110, 263004 (2013).
 - [19] Budker, D. & Romalis, M. Optical magnetometry. *Nature Phys.* 3, 227–234 (2007).
 - [20] Dang, H. B., Maloof, A. C. & Romalis, M. V. Ultrahigh sensitivity magnetic field and magnetization measurements with an atomic magnetometer. *Appl. Phys. Lett.* 97, 151110 (2010).
 - [21] Jau Y.Y., Post A.B., Kuzma N.N., Braun A.M., Romalis M.V. & Happer W. Intense, narrow atomic-clock resonances. *Phys. Rev. Lett.* 92, 110801 (2004).
 - [22] Happer W., Jau Y. Y. & Walker T. Optically pumped atoms. 159–218 (WILEY-VCH Press, 2010).
 - [23] Schori, C., Julsgaard, B., Sørensen, J. L. & Polzik, E. S. Recording quantum properties of light in a long-lived atomic spin state: Towards quantum memory. *Phys. Rev. Lett.* 89, 057903 (2002).
 - [24] Neveu P., Maynard M. A., Bouchez R., Lugani J., Ghosh R., Bretenaker F., Goldfarb F. & Brion E. Coherent Population Oscillation-Based Light Storage. *Phys. Rev. Lett.* 118, 073605 (2017).
 - [25] Rochester S.M., Hsiung D.S., Budker D., Chiao R.Y., Kimball D.F. & Yashchuk V.V. Self-rotation of resonant elliptically polarized light in collision-free rubidium vapor. *Phys. Rev. A* 63, 043814 (2001).
 - [26] Li, W., Balabas, M., Peng X., Pustelny, S., Wickenbrock, A., Yang Y., Guo H. & Budker, D. Investigation of antirelaxation wall coatings beyond melting temperatures," 2017 Conference on Lasers and Electro-Optics (CLEO), San Jose, CA, 2017, pp. 1-2.
 - [27] Walker, T. G. & Happer, W. Spin-exchange optical pumping of noble-gas nuclei. *Rev. Mod. Phys.* 69, 629–642 (1997).
 - [28] Haroche, S. & Cohen-Tannoudji, C. Resonant transfer of coherence in nonzero magnetic field between atomic levels of different g factors. *Phys. Rev. Lett.* 24, 974 (1970).
 - [29] Katz, O., Peleg, O. & Firstenberg, O. Coherent coupling of alkali atoms by random collisions. *Phys. Rev. Lett.* 115, 113003 (2015).
 - [30] Kornack, T. W. & Romalis, M. V. Dynamics of two overlapping spin ensembles interacting by spin exchange. *Phys. Rev. Lett.* 89, 253002 (2002).
 - [31] Firstenberg, O., Shuker M., Pugatch R., Fredkin D. R., Davidson N. & Ron A. Theory of thermal motion in electromagnetically induced transparency: Diffusion, Doppler, Dicke and Ramsey. *Phys. Rev. A* 77, 043830 (2008).

Supplementary Information for “Light storage for one second at room temperature”

In this Supplementary Information, we analytically derive the mapping from light to atoms $\eta_L e^{i\phi_L} \rightarrow \eta_A e^{i\phi_A}$ (Sec. I) and from atoms to light $\eta_A e^{i\phi_A} \rightarrow \eta_L^{\text{out}} e^{i\phi_L^{\text{out}}}$ (Sec. II). Subsequently, we examine the overall mapping between the input and output signals and present a method to eliminate its ellipticity (Sec. III).

I. Storage: mapping light to atoms

In light storage based on EIT, the atomic state during storage corresponds to the EIT dark state. Here we derive the dark state by analyzing the non-Hermitian Hamiltonian of the system [S1]. For our $\Delta m = 1$ scheme, the control field E_c and signal field E_s comprise the total electric field as

$$\vec{E} = E_c \hat{z} + E_s \hat{y} = E_c (\hat{z} + i\eta_L e^{i\phi_L} \hat{y}). \quad (\text{S1})$$

In principle, the ground level of the Cs atoms have many spin states that are coupled by the signal and control fields. However, we use optical pumping to initialize the atoms in the maximally polarized state $|g\rangle$ (see Fig. 1 in the main text), while the weak signal field with $\eta_L \ll 1$ varies this state only perturbatively. We therefore consider here, in addition to $|g\rangle$, only the states $|r\rangle, |e\rangle, |p\rangle$, which couple to $|g\rangle$ to first order in η_L . The non-Hermitian Hamiltonian is given by $H = H_0 + V$, where

$$\begin{aligned} H_0 &= -i\Gamma |e\rangle \langle e| + (\Delta - i\Gamma) |p\rangle \langle p| \\ V &= \Omega_s |g\rangle \langle e| + \Omega_c |r\rangle \langle e| + a_{cs} \Omega_c |g\rangle \langle p| + b_{cs} \Omega_s |r\rangle \langle p| + \text{h.c.} \end{aligned} \quad (\text{S2})$$

Here $\Delta = 1100 \cdot 2\pi$ MHz is the excited-level hyperfine splitting, and we take $\Gamma = 124 \cdot 2\pi$ MHz for the half linewidth of the Doppler-broadened optical transition. The Rabi frequencies are given by $\Omega_c = d_{cs} |E_c| / (\sqrt{2}\hbar)$ and $\Omega_s = \sqrt{2}\Omega_c \eta_L e^{i\phi_L}$, where $d_{cs} = 2.6 \cdot \frac{\sqrt{7}}{4} ea_0$ is the dipole moment transition element for the Cs D1 transition, with the electron charge e and Bohr radius a_0 [S3]. The ratios of the Clebsch-Gordan coefficients between the two Λ systems is $a_{cs} = 4/\sqrt{7}$ and $b_{cs} = 1/\sqrt{7}$.

Because of the off-resonant coupling to the state $|p\rangle$, the system has no dark state, as manifested by the fact that H has no zero eigenvalues. However, one can identify a “quasi-dark” state — the eigenstate of H with the lowest imaginary eigenvalue. For our Hamiltonian, the lowest imaginary eigenvalue $\lambda_{\min} \propto -i\Gamma\Omega_c^2/\Delta^2$ accounts for the loss of population from the dark state to other ground-level states via off-resonant pumping. Diagonalizing H , we find the corresponding eigenstate to first order in η_L and in Γ/Δ ,

$$|\psi_A\rangle = |g\rangle + \sqrt{2}\eta_L e^{-3i\alpha} [e^{i(\phi_L - \alpha)} \underbrace{-i\alpha e^{-i(\phi_L - \alpha)}}_{\text{perturbation to the ideal dark state}}] |r\rangle \quad (\text{S3})$$

with $\alpha = f_{cs}\Gamma/\Delta$, and $f_{cs} = 0.58$ is a constant derived from the Clebsch-Gordan coefficients. To relate this state to the Bloch sphere representation, we write it as

$$|\psi_A\rangle = |g\rangle + \sqrt{2}\eta_A e^{i\phi_A} |r\rangle \quad (\text{S4})$$

and identify the Bloch spin quadratures

$$s_x = \frac{1}{2}\eta_A \cos(\phi_A); \quad s_y = \frac{1}{2}\eta_A \sin(\phi_A); \quad s_z = \frac{1}{2}.$$

The parameters η_A and ϕ_A thus serve as the angles on the Bloch sphere. With $\alpha \neq 0$, the state (S3) manifests a non-ideal mapping from the Poincaré sphere to the Bloch sphere. From Eqs. (S4) and (S3), we find the $\eta_L e^{i\phi_L} \rightarrow \eta_A e^{i\phi_A}$ mapping

$$\eta_A = \eta_L \sqrt{1 - 2\alpha \sin(2(\phi_L - \alpha))} \quad (\text{S5})$$

and

$$\phi_A = -\frac{\pi}{4} - 3\alpha + \arctan \left[\frac{1 - \alpha}{1 + \alpha} \tan \left(\phi_L + \frac{\pi}{4} - \alpha \right) \right]. \quad (\text{S6})$$

These are the mathematical equations of an ellipse with the semi-major and semi-minor axes $\eta_L (1 \pm \alpha)$ rotated by an angle $(\frac{\pi}{4} - \alpha)$. Mathematically, the phase ϕ_L serves as the eccentric anomaly of the ellipse in the Bloch sphere. The mapping is exemplified graphically in Fig. S1 for $\eta_L = 10^{-3}$ and $\alpha = 0.1$ with $0 \leq \phi_L \leq 2\pi$. The ellipticity of the mapping, determined by the parameter α , is manifested by a dependence of the tilt angle of the spin on the azimuthal phase.

As expected, in the ideal case $\alpha \rightarrow 0$ (for $\Gamma \ll \Delta$), the quasi-dark state in Eq. (S3) becomes the ideal dark state, and Eqs. (S5) and (S6) reduce to the simple linear relations $\eta_A = \eta_L$ and $\phi_A = \phi_L$.

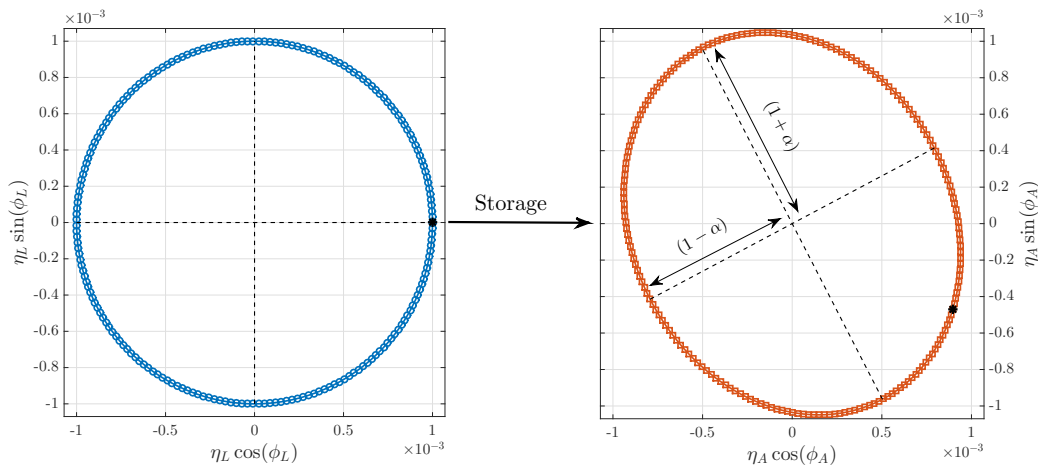


Figure S1. Mapping of the light state to atomic spin state ($\eta_L = 10^{-3}$, $\alpha = 0.1$). We mark the points $\phi_L = 0$ and $\phi_A(\phi_L = 0)$ (black asterisks) to illustrate the transformation of the azimuthal phase, which acquires a mean additional phase shift of -3α .

II. Retrieval: mapping atoms to light

The retrieval process could be described as the reverse process of storage [S4, S5]. Nevertheless, it is instructive to consider a complementary formalism, which we give in this section. During the retrieval of the signal, similarly to storage, the atomic excitation changes adiabatically the incoming light field (control only) to a new light field (control+signal) that minimizes the loss. A formalism for describing the propagation of the electric field through the medium was introduced by Happer *et al.* [S6]. They write the propagation equation of the field amplitude \vec{E} as

$$\frac{d}{d\tilde{x}} \vec{E} = 2\pi i k n \langle \hat{\chi} \rangle_{\perp} \vec{E}, \quad (\text{S7})$$

where k is the wave-number of the laser, n is the atomic density, and $\tilde{x} = x - ct$ is the transformed spatial coordinate of the pulse. This equation relates the electric field vector in the medium $\vec{E} = (E_y, E_z)$ to the atomic state $|\psi_A\rangle$ using the mean transverse susceptibility tensor of the atoms $\langle \hat{\chi} \rangle_{\perp} = \langle \psi_A | \hat{\chi} | \psi_A \rangle_{\perp}$, where $\chi_{ij} = d_i d_j / (\Delta - i\Gamma)$ is the atomic susceptibility operator, and d_i are the atomic dipole operators. The subscript “ \perp ” denotes the reduced

2×2 operator, describing the yz polarization plane [S7]. We identify the retrieved light field as the eigenvector of $\langle \vec{\chi} \rangle_{\perp}$ with minimal imaginary eigenvalue, that is, the light field with minimal loss [S8]. Using the atomic state (S4), the susceptibility tensor of the medium is given by

$$\langle \vec{\chi} \rangle_{\perp} = i \frac{d_{Cs}^2}{\Gamma} \begin{pmatrix} 1 - 2ib_{Cs}^2 \frac{\Gamma}{\Delta} \eta_A & -i\eta_A (e^{i\phi_A} - ia_{Cs}b_{Cs} \frac{\Gamma}{\Delta} e^{-i\phi_A}) \\ i\eta_A (e^{-i\phi_A} - ia_{Cs}b_{Cs} \frac{\Gamma}{\Delta} e^{i\phi_A}) & \eta_A - \frac{i}{2} a_{Cs}^2 \frac{\Gamma}{\Delta} \end{pmatrix}. \quad (S8)$$

The least decaying eigenvector \vec{E}^{out} of this matrix is given to first order in η_A and in Γ/Δ by

$$\vec{E}^{\text{out}} = \begin{pmatrix} i\eta_A e^{-i2\alpha} (e^{i\phi_A} - i\alpha e^{-i\phi_A}) \\ 1 \end{pmatrix}. \quad (S9)$$

The resulting light field is elliptically polarized. We can relate the polar and azimuthal angles on the Poincaré sphere to those of the Bloch sphere by

$$\eta_L^{\text{out}} = \eta_A \sqrt{1 - 2\alpha \sin(2\phi_A)} \quad (S10)$$

and

$$\phi_L^{\text{out}} = \frac{\pi}{4} - 2\alpha + \arctan \left[\frac{1 + \alpha}{1 - \alpha} \tan \left(\phi_A - \frac{\pi}{4} \right) \right]. \quad (S11)$$

Once again, these are the mathematical equations of an ellipse with the semi-major and semi-minor axes $\eta_L (1 \mp \alpha)$, now rotated by an angle $\frac{\pi}{4}$. The mapping is exemplified graphically in Fig. S2 for $\eta_A = 10^{-3}$ and $\alpha = 0.1$ with $0 \leq \phi_A \leq 2\pi$. The ellipticity of the mapping, determined by the parameter α , tilts the light polarization differently for different azimuthal phases.

Here again, in the ideal case $\alpha \rightarrow 0$, the medium becomes completely transparent to the state \vec{E}^{out} , and Eqs. (S10) and (S6) reduce to the simple linear relations $\eta_L^{\text{out}} = \eta_A$ and $\phi_L^{\text{out}} = \phi_A$.

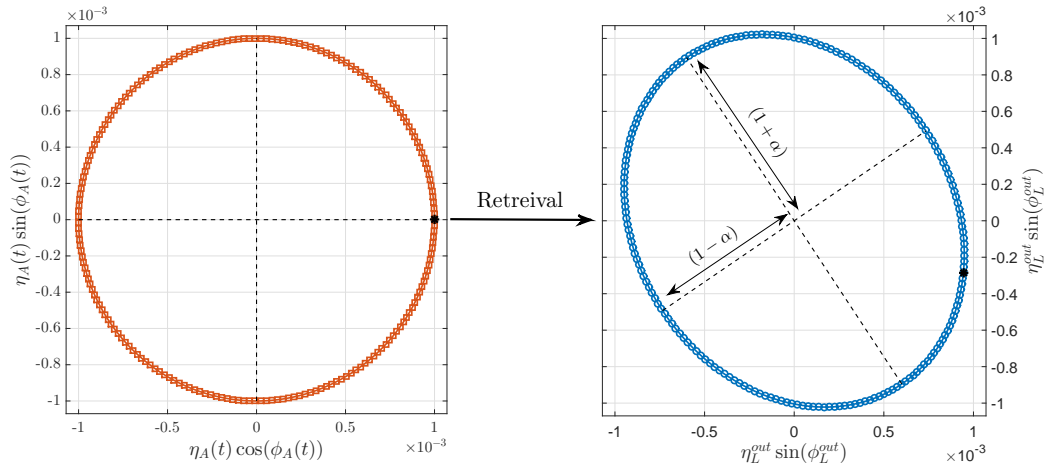


Figure S2. Mapping of the atomic spin state to the light state when retrieving the signal ($\eta_A = 10^{-3}$, $\alpha = 0.1$). We mark the points $\phi_A = 0$ and $\phi_L (\phi_A = 0)$ (black asterisk) to illustrate the mapping of the azimuthal phase, which acquires a mean additional phase shift of -2α .

III. Protocol for eliminating the ellipticity of the overall storage-to-retrieval transformation

The overall transformation of the storage, followed by a storage time t , and then retrieval, is described by

$$\eta_L \rightarrow \eta_A(0) \rightarrow \eta_A(t) \rightarrow \eta_L^{\text{out}}, \quad (\text{S12})$$

$$\phi_L \rightarrow \phi_A(0) \rightarrow \phi_A(t) \rightarrow \phi_L^{\text{out}}. \quad (\text{S13})$$

The first and third steps are given by Eqs. (S5), (S6), (S10), and (S11). The second step describes the dynamics of the atomic spins in the dark for a duration t , governed by a Larmor precession,

$$\phi_A(t) = \phi_A(0) + \omega_B t, \quad (\text{S14})$$

and by decay due to the various relaxation mechanisms,

$$\eta_A(t) = \eta_A(0)e^{-t/\tau_s}.$$

Ideally $\alpha = f_{cs}\Gamma/\Delta \ll 1$ and $t \ll \tau_s$, such that Eqs. (S10) and (S11) are the inverse transformation of Eqs. (S5) and (S6), and the ground state relaxation is negligible, yielding perfect storage and retrieval of light. However, if $\alpha < 1$ but non-negligible (as in our experiment), then the retrieved signal is altered by the coupling to the off-resonant level $|p\rangle$ and given to first order in α by

$$\phi_L^{\text{out}} \approx \phi_L + \omega_B t - 6\alpha - 2\alpha \cos(\omega_B t - 3\alpha) \cos(2\phi_L + \omega_B t) \quad (\text{S15})$$

$$\eta_L^{\text{out}} \approx \eta_L e^{-t/\tau_s} (1 - 2\alpha \sin(2\phi_L + \omega_B t) \cos(\omega_B t - 3\alpha)). \quad (\text{S16})$$

We see that, in general, the output light suffers the elliptical distortion twice, resulting in a storage efficiency that depends on the phase. This effect can be understood either as self rotation of the light polarization [S9] or as arising from degenerate four-wave mixing [S10].

The elliptical distortion can be removed completely by setting the magnetic field to satisfy $\omega_B t \approx 3\alpha - \pi/2$, see Fig. S3. For this value, the transformation simplifies to $\phi_L^{\text{out}} \approx \phi_L - 6\alpha$ and $\eta_L = e^{-t/\tau_s} \eta_L$, such that the amplitude η_L is independent of ϕ_L . We emphasize that the distortion is eliminated for all orders of α and is thus completely removed. The process can be described in terms of a perfect “quantum eraser”, since it neither depends on the (intermediate) spin states nor it involves any classical feedback or measurement of the quantum system.

* Corresponding author: or.katz@weizmann.ac.il

- [S1] Non-Hermitian Hamiltonian dynamics with stochastic quantum jumps is used to solve open-systems dynamics [S2]. In EIT, population of the excited state is avoided, thus the effect of the quantum jumps in determining the dark state is small.
- [S2] Fleischhauer, M., Imamoglu, A. & Marangos, J. P. Electromagnetically induced transparency: Optics in coherent media. *Rev. Mod. Phys.* 77, 633–673 (2005).
- [S3] Steck, D. A. <http://steck.us/alkalidata> (2009).
- [S4] Novikova, I., Gorshkov A. V., Phillips D. F., Sørensen A. S., Lukin M. D. and Walsworth R. L., Optimal Control of Light Pulse Storage and Retrieval, *Phys. Rev. Lett.*, 98, 243602 (2007).
- [S5] Nunn J., Reim K., Lee K. C., Lorenz V. O., Sussman B. J., Walmsley I. A. and Jaksch D., Multimode Memories in Atomic Ensembles, *Phys. Rev. Lett.* 101, 260502 (2008).
- [S6] Happer W., Jau Y. Y. & Walker T. *Optically pumped atoms*. 159–218 (WILEY-VCH Press, 2010).
- [S7] B. S. Mathur, H. Y. Tang, and W. Happer, *Phys. Rev. A* 2, 648 (1970).
- [S8] When identifying the atomic quasi-dark state in the analysis of the storage process, we assumed time-invariant light fields Ω_c and Ω_s . To identify the least decaying mode of the light, we correspondingly take a time-invariant (steady-state) atomic susceptibility $\langle \hat{\chi} \rangle$.
- [S9] Novikova, I., Phillips, D. F. & Walsworth, R. L. Slow light with integrated gain and large pulse delay *Phys. Rev. Lett.* 99, 173604 (2007).
- [S10] Xu, X., Shen, S. & Xiao, Y. Tuning the phase sensitivity of a double-lambda system with a static magnetic field. *Opt. Exp.* 21, 11705 (2013).

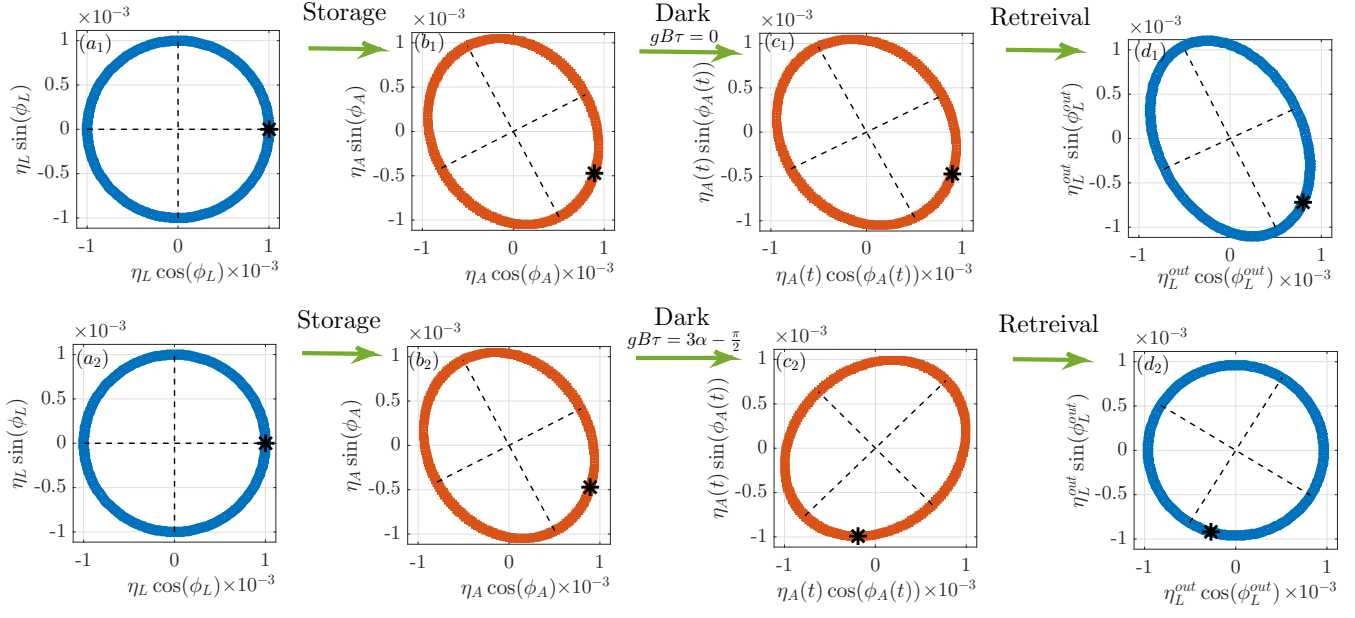


Figure S3. Full transformation from storage to retrieval ($\eta_L = 10^{-3}$ and $\alpha = 0.1$). (a1)-(d1): For a vanishing Larmor precession $\omega_B t = 0$, the transformation is elliptical. (a2)-(d2): For $\omega_B t = 3\alpha - \pi/2$, the elliptical distortion is eliminated.